

Received June 22, 2020, accepted July 5, 2020, date of publication July 9, 2020, date of current version July 22, 2020.

Digital Object Identifier 10.1109/ACCESS.2020.3008214

Design and Vibration Optimization of Direct Current Motor of Permanent Magnet of Rectangular Magnetic Steel

KAI HU^{1,2} AND GUANGMING ZHANG¹

¹College of Electrical Engineering and Control Science, Nanjing Tech University, Nanjing 211816, China

²Nanjing Institute of Agricultural Mechanization, Ministry of Agriculture and Rural Affairs, Nanjing 210014, China

Corresponding author: Guangming Zhang (869507113@qq.com)

This work was supported in part by the Research and Development Project of Jiangsu Province under Grant BE2017164, in part by the Research and Development Program of Chinese Academy of Agricultural Sciences under Grant CAAS-NRAM-SJ-201903, and in part by the Scientific Research Project of Nanjing Research Institute for Agricultural Mechanization Ministry of Agriculture and Rural Affairs under Grant S201907.

ABSTRACT Direct current motor of permanent magnet (PMDCM) is widely used at present. To optimize its operating performance and vibration characteristics, a new PMDCM of rectangular magnetic steel was developed. The co-simulation was conducted based on RMxprt and MAXWELL. The simulation results verify that the output power and torque meet the design requirements. Then the cogging torque of the designed motor was analyzed and optimized by using response surface method. The influence degree of each factor on cogging torque was analyzed. When factor A, the factor B, and factor C are 33.51mm, 2.42mm, and 1.50mm, the root-mean-square (RMS) value and the maximum value of the cogging torque are smallest. The fitting accuracy of the two regression equations of RMS and maximum cogging torque is 94.30% and 97.26%. To further verify the correctness of analysis results, the optimized motor and reference motor were manufactured and the vibration velocity data at different positions were measured. The measured data shows that the maximum and average data of vibration velocity at measuring point 1 are decreased by 18.99% and 19.03% and the maximum and average vibration velocity at measuring point 2 are decreased by 9.73% and 4.70%. The method of vibration reduction is effective. The proposed optimization scheme and method may be extended to other motor for reducing vibration.

INDEX TERMS Co-simulation, cogging torque, PMDCM, response surface method, vibration optimization.

I. INTRODUCTION


A. RESEARCH BACKGROUND

The direct current motor of permanent magnet (PMDCM) not only has the linear regulation characteristics and wide speed range, but also has the advantages of small size, high efficiency, simple structure and reliable [1]–[3]. If the PMDCM is equipped with a speed stabilizer, it can also be applied to the occasions where the rotation speed needs to be stable even if the voltage fluctuates. Therefore, PMDCM has been extensively employed in household appliances, machinery, power tools, medical equipment and so on [4]–[7].

There are various shapes of magnetic steel for PMDCM. In the past, the permanent magnetic steel shape was always cylindrical. However, the manufacturing processing

of cylindrical magnetic steel is difficult, and the manufacturing cost is even higher than the cost of the permanent magnet [8]. In addition, the cylindrical magnetic steel of PMDCM is often pasted on the rotor surface. Due to the large centrifugal force of high-speed motor and the low structural strength of the pasted magnetic steel, it is necessary to install permanent magnet sheaths on the medium and high-speed motors [9]–[12]. In order to avoid the above problems, permanent magnets have been processed into rectangular structures as much as possible in recent years, and installed in an embedded manner. The design and optimization of the PMDCM with inner rectangular permanent magnet have attracted many attentions.

At the same time, vibration analysis and optimization of PMDCM have been become another hot topic in this research field. Previous literature studies show that the vibration of PMDCM is mainly divided into mechanical vibration and

The associate editor coordinating the review of this manuscript and approving it for publication was Ning Sun .

electromagnetic vibration [13]–[16]. Mechanical vibration mainly comes from brush, bearing and eccentric motion of rotor, and the suppression techniques of mechanical vibration have been adequately developed. Electromagnetic vibration is primarily caused by the electromagnetic force operating on the stator. It not only affects the accuracy of torque control, but also aggravates the vibration and noise of the motor [17], [18].

B. LITERATURE REVIEW

Only permanent magnet motors have cogging torque which is generated by the interaction between the armature winding core and the permanent magnetic steel when the windings are not energized. The cogging torque is complicated which is affected by various factors such as magnetic steel structure, pole slot coordination, inclined groove, inclined pole, pole arc coefficient, etc. Therefore there is no mature theory to optimize the cogging torque. Jiajie Zou proposed a method to optimize the cogging torque and the distortion rate of electromotive force based on genetic algorithm [19]. A new optimization method for vibration and noise of motor by optimizing arc coefficient was put forward Wan [20]. Zhiyu Chen deduced the cogging torque of permanent magnet synchronous motors with different integer slot and pointed out that the different integer slots have different cogging torque amplitude and different effects on the low-speed operating performance [21]. But the research is unable to encompass how to reduce cogging torque by optimized relevant parameters. Tarczewski T and Grzesiak L M have proved that electromagnetic noise is not only related to the radial electromagnetic force, but also to the stator mode [22]. Giirkan Zenginobuz analyzed the mechanism of torque generation of permanent magnet motor and proposed two control strategies to reduce torque fluctuation. The first strategy is based on the finite element method to calculate the modulating current, and the second strategy is the on-line torque estimation [23]. Colamartino F and Jian achieved the minimum transient current parameters by optimizing the motor current waveform and finally obtained a better transient cogging torque [24], [25]. The literature studies show that a large number of researches have been carried out on the cogging torque in previous studies, but the influence degree of magnetic steel parameters of PMDCM on the cogging torque and vibration characteristics has not been clarified. Previous studies also have failed to consider the influence of cogging torque on vibration characteristics of motor at different positions.

C. PAPER ORGANIZATION

The remaining parts of the paper are organized as follows: The main parameters of the new PMDCM with rectangular magnetic steel were designed in Section I. The co-simulation was conducted based on RMxpRT and MAXWELL in Section II. The analysis and optimization of cogging torque by using response surface method was expounded in Section III. And the vibration measuring experiment of optimized motor and reference motor was carried out

TABLE 1. Main design parameters of the motor.

Parts	Parameters	Value
Stator	Outer diameter	70mm
	Inner diameter	35mm
	Length	70mm
	Number of slots	12
Rotor	Outer diameter	34mm
	Inner diameter	15mm
	Length	70mm
	Poles	4

in Section IV. At last, the concluding remarks of this study were described in Section V.

II. DESIGN OF PMDCM OF RECTANGULAR MAGNETIC STEEL

The PMDCM of rectangular magnetic steel with rated power of 300W and rated speed of 1800rpm was developed. After referring to the Motor Design Manual and empirical Formula 1, the main dimensions of the motor were determined. The main design parameters of the motor are listed in Table 1.

$$\frac{4T}{\pi D_R^2 L} = 2\sigma \quad (1)$$

T is denoted as the rated output torque and D_R presents the outer diameter of the rotor. The length of the motor core is denoted as L . σ is the shear stress on the rotor surface, and its value range is 2-5 lbf/in².

III. CO-SIMULATION OF RMxpRT AND MAXWELL

A. SIMULATION MODEL ESTABLISHMENT

The dimensional parameters, control mode, winding type, magnetic steel size, etc. were defined in the RMxpRT software. The silicon steel sheet and magnetic steel were chosen as M19_24G and XG196/96 respectively. And then the performance parameters of the designed motor were calculated in RMxpRT, and the motor power and torque curves are presented in Fig.1. At the rated speed of 1800rpm, the output power is 302.8W and the output torque is 1.61N·m. The simulation results show that the motor parameters are correct.

To further research the distribution of magnetic field, the model established in RMxpRT was imported into MAXWELL for co-simulation. The 1/4 motor model was adopted for improving the calculation efficiency. Two kinds of boundary conditions of master-slave and vector-potential were employed. The master-slave boundary aims to simplify the geometric model by calculating only one pole or a pair of poles. The vector-potential boundary is imposed on the edge of the solution domain or the calculation model. Then the motor model was meshed. In order to obtain higher calculation accuracy and smooth magnetic induction intensity (MI) curves, the meshing size of stator and other rotating parts is set to 2mm and 0.5mm respectively. The finite element model

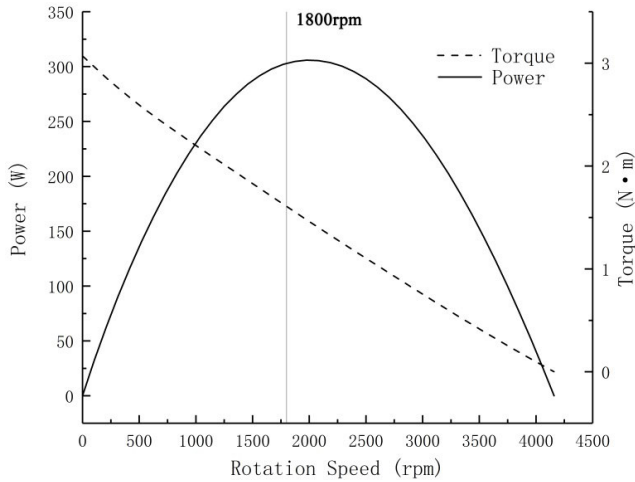


FIGURE 1. The output power and torque at different rotation speed.

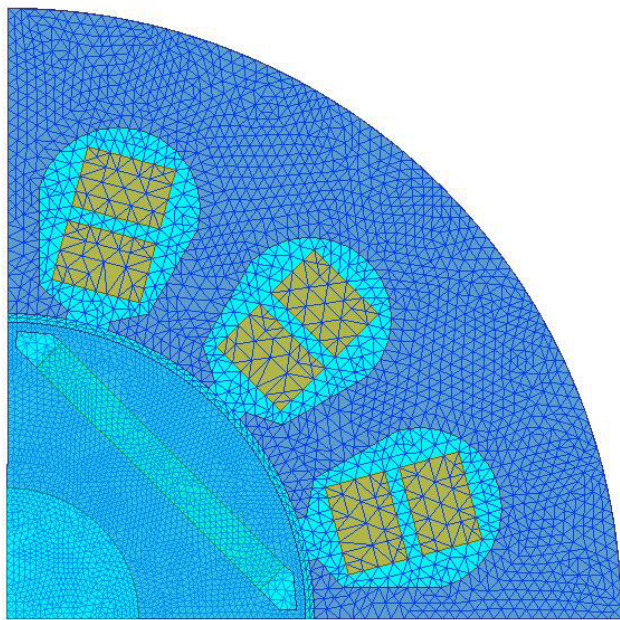


FIGURE 2. The finite element model.

in MAXWELL is shown in the Fig.2. The total numbers of meshes are 18105. The power excitation of the motor is driven by the external circuit which was designed in the Simpler software. And the field-circuit coupling analysis of the magnetic field was carried out. The designed external circuit is shown in Fig.3.

B. TRANSIENT MAGNETIC FIELD SIMULATION

The motor operates at the rated rotation speed and the mechanical characteristics of the load are simplified in MAXWELL simulation. The total simulation time is 40ms. The maps of MII at 10ms, 20ms, 30ms and 40ms are shown in Fig.4 respectively.

It can be illustrated from Fig.4 that the MII of each part is reasonable. The MII of the stator tooth and yoke ranges

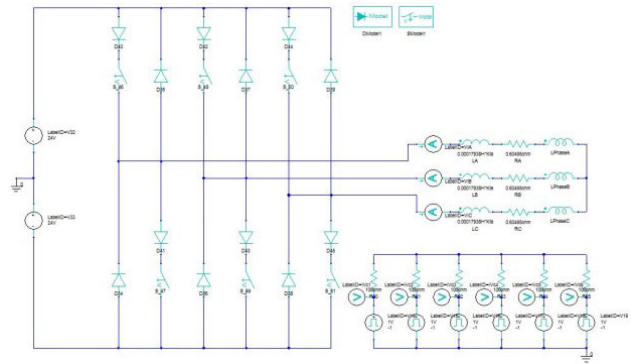


FIGURE 3. The external circuit.

from 0.9T to 1.6T. The MII of the magnetic isolation bridge is larger. This means that most magnetic energy enters the stator from the rotor through the air gap and only a small amount of magnetic energy passes from the N pole to the adjacent S pole through the magnetically isolated bridge. The MII of each position at different time is not more than 2.35T which is less than the saturation value of MG19_24 material.

In order to further explore the internal magnetic field of the motor, the MII at three points was observed. The positions of the three points are shown in Fig.5, and the MII of each point is given in Fig.6. The MII of the three points change periodically and the cycle time is 8.33ms. The change of MII in the first cycle is slightly different from that in the subsequent cycles, because the motor has not yet reached a stable state. Point 1 is placed at the outer circle of the stator, and its MII is relatively small. Its maximum value does not exceed 1.5T. Point 2 is located in the stator teeth, and its maximum MII is about 1.85T. Point 3 is located at the magnetic isolation bridge of the rotor, and its MII value fluctuates greatly. The maximum value of MII at point 3 is about 2.1T.

IV. VIBRATION OPTIMIZATION

A. COGGING TORQUE ANALYSIS

Cogging torque is a unique phenomenon of permanent magnet motors, and it is defined as the torque generated by the interaction between the armature winding core and the permanent magnet when the winding is not energized. Cogging torque is one of the main factors causing vibration.

Cogging torque can be calculated by

$$T_{cog} = - \frac{\partial W}{\partial \alpha} \tag{2}$$

T_{cog} is denoted as cogging torque. W is the field energy when the motor is not energized and α is the relative angle between stator and rotor.

If the core permeability is infinite, the energy of the motor can be calculated approximately by

$$W = \frac{1}{2\mu_0} \int_v B_r^2(\theta) \left[\frac{h_m(\theta)}{h_m(\theta) + \delta(\theta, \alpha)} \right]^2 dv \tag{3}$$

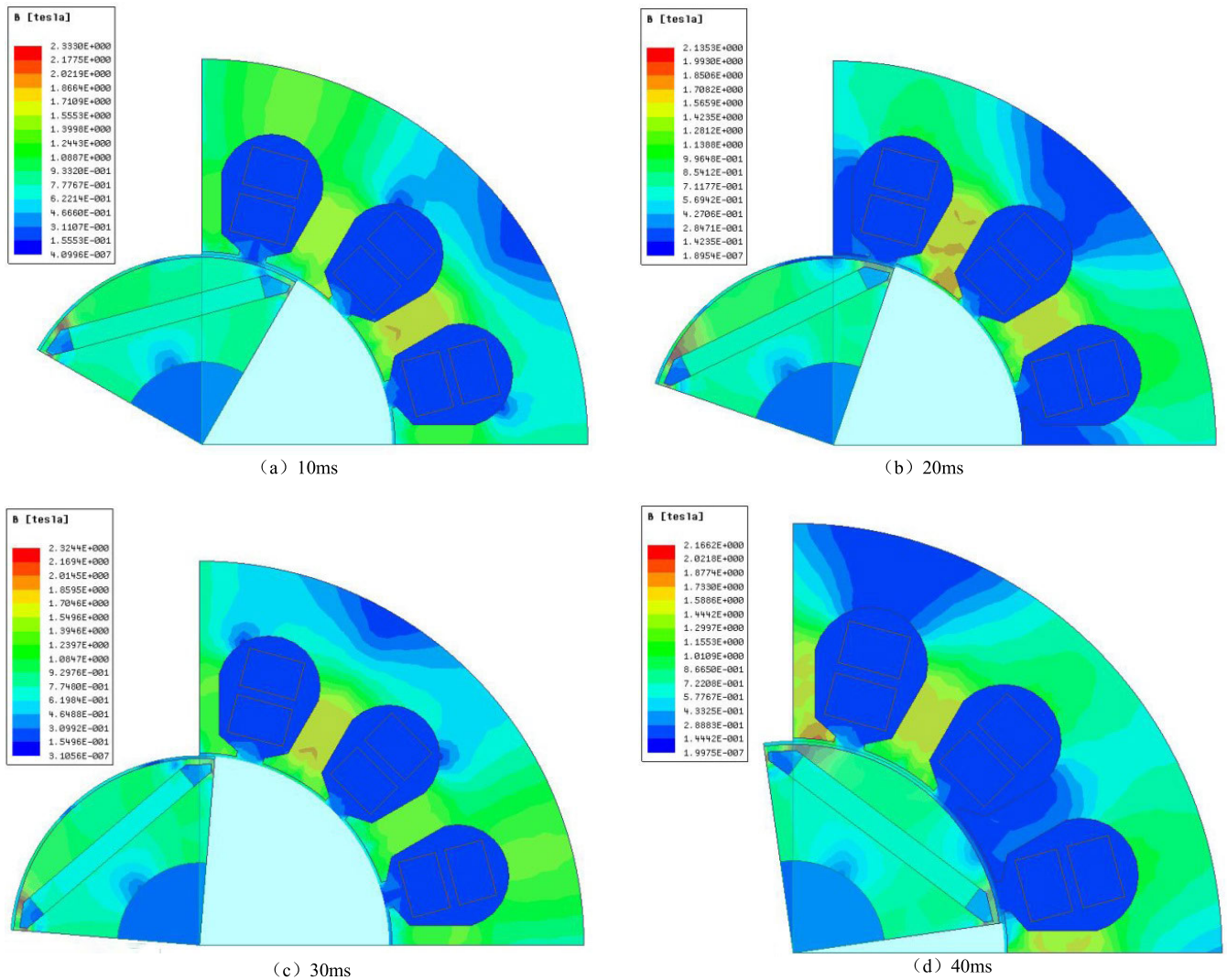


FIGURE 4. The MII maps at different time.

The air gap permeability, air gap volume, torque angle and permanent magnet remanence are μ_0 , V , θ and $B_r^2(\theta)$ respectively. The $h_m(\theta)$ is the magnetizing length of the magnetic steel in the circumferential direction and $\delta(\theta, \alpha)$ is effective air gap length.

Fourier operations on $B_r^2(\theta)$ and $\left[\frac{h_m(\theta)}{h_m(\theta)+\delta(\theta, \alpha)}\right]^2$ are carried out. The calculation results are shown as follows.

$$B_r^2(\theta) = B_{r0} + \sum_{n=1}^{\infty} B_{rn} \cos(2np\theta) \quad (4)$$

$$\left[\frac{h_m(\theta)}{h_m(\theta)+\delta(\theta, \alpha)}\right]^2 = G_0 + \sum_{n=1}^{\infty} G_n \cos(nZ(\theta + \alpha)) \quad (5)$$

In these equations, the B_{r0} , B_{rn} , G_0 , G_n are corresponding Fourier coefficients. The specific forms of G_0 and G_n are related to the distribution function of the air gap. The numbers of slots and poles are denoted as Z and p .

The Formula 6 can be deduced by integrating Formula 2, Formula 4 and Formula 5.

$$T_{cog} = \frac{\pi Z L_{ef}}{4\mu_0} (R_{out}^2 - R_{in}^2) \sum_{n=1}^{\infty} n G_n B_r \frac{nZ}{2p} \sin(nZ\alpha) \quad (6)$$

R_{out} and R_{in} are outer radius of the stator and inner radius of the rotor respectively. L_{ef} is axial length of the motor armature and n is an integer. The value of n should ensure that $\frac{nZ}{2p}$ is an integer.

It can be illustrated from above analysis that the cogging torque of the permanent magnet motor is closely related to the geometric parameters of the motor and the magnetic steel. Therefore the relevant parameters can be optimized to decrease the cogging torque and reduce the vibration.

B. OPTIMIZATION FACTORS

The cogging torque optimization was performed under the premise that the rated power of the motor is

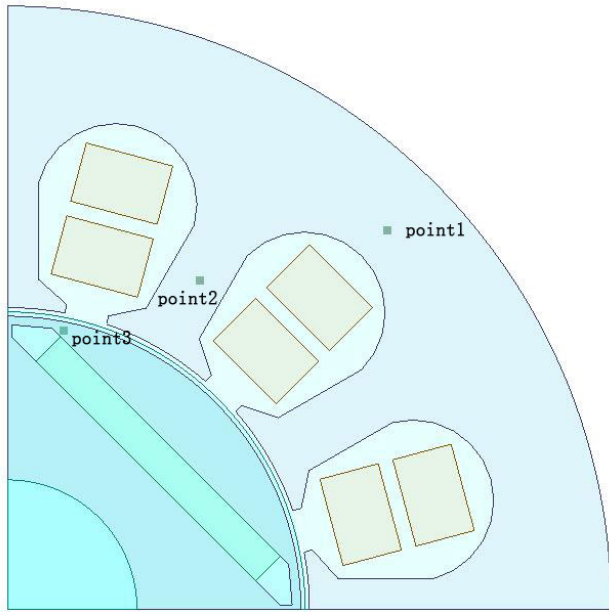


FIGURE 5. The positions of the selected three points.

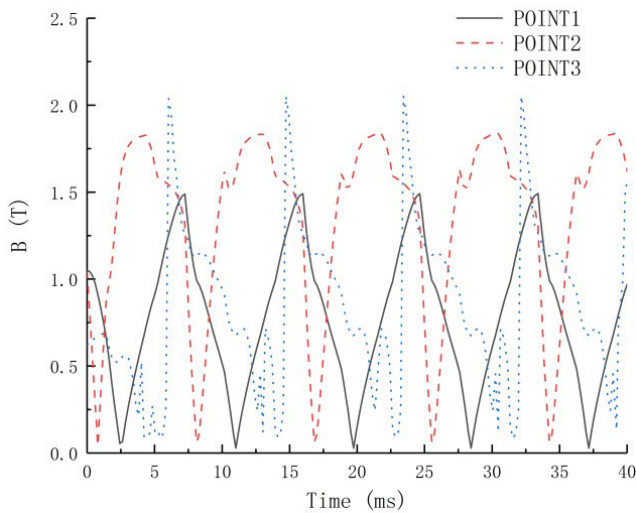


FIGURE 6. The MII of selected three points.

basically unchanged. That means the dimensions of the stator, rotor and permanent magnets should not be modified. The air gap length (factor A), the distance between the magnetic isolation bridge and the outer circle of the rotor (factor B), and the distance between two magnetic isolation bridges (factor C) were chosen as the optimization factors. The 3 factors are presented in Fig.7. The root-mean-square (RMS) value and maximum value of the cogging torque is confirmed as the optimization target parameters. The RMS of cogging torque can be calculated by

$$RMS_{cog} = \sqrt{\frac{\sum_{i=1}^n T_{cog-i}^2}{n}} \quad (7)$$

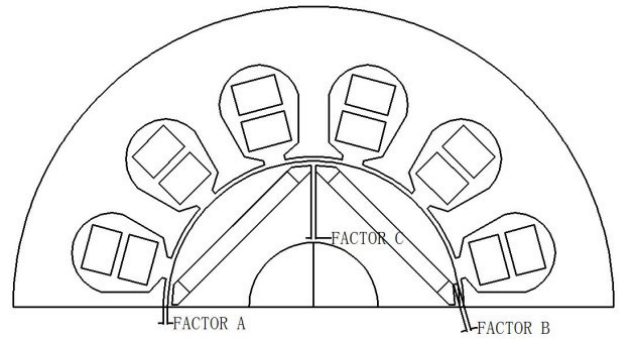


FIGURE 7. Schematic diagram of 3 factors.

RMS_{cog} is the RMS of cogging torque. T_{cog-i} is the cogging torque value at point i and n is the total number of points in a cycle.

C. RESPONSE SURFACE OPTIMIZATION

The mathematical relationship between the optimization objective and the influencing factors is unknown. The basic theory of response surface optimization is to build a mathematical model to estimate the total number with a limited number of experiments. The system model can be expressed by

$$y = f(x_1, x_2, x_3 \dots x_n) \quad (8)$$

y is the dependent variable and x_n is the n independent variable.

Then Formula 9 can be obtained by performing Taylor expansion on Formula 8.

$$y \approx f(0) + \frac{f'(0)}{1!}x + \frac{f''(0)}{2!}x^2 + \dots + \frac{f^n(0)}{n!}x^n \quad (9)$$

It can be indicated from Formula 9 that dependent variables can be fitted by different order regression equations. This is the basic theory of response surface optimization. Box-behnken model is adopted for response surface analysis in this paper. Response surface experiment design and calculation results are shown in Table 2.

It is apparent from Table 2 that the cogging torque is the smallest in the second group (Factor A, factor B, and factor C are 33.5mm, 2.50mm, and 2.00mm.). The RMS value and maximum value of cogging torque is 93.76mN·m and 165.63mN·m respectively. The regression equations of RMS value and maximum value of cogging torque shown in Formulas 10 and 11 are fitted by the quadratic regression analysis method. The fitting accuracy of the two regression equations is 94.30% and 97.26%.

$$T_{cog-RMS} = -42965.21842 + 2514.71421A + 136.11289B - 17.5C - 6.36AB + 10BC - 36.58947A^2 + 8.97053B^2 \quad (10)$$

$$T_{cog-max} = -116746 + 6837.09855A + 302.93697B - 17.5C - 12.25AB + 10BC - 99.75737A^2 + 11.90263B^2 \quad (11)$$

TABLE 2. Response surface experiment design and calculation results.

Group	Factor A /mm	Factor B /mm	Factor C /mm	The RMS of cogging torque (mN·m)	The maximum of cogging torque (mN·m)
1	34.00	2.50	1.50	103.98	194.25
2	33.50	2.50	2.00	93.76	165.63
3	34.50	1.50	2.00	131.33	237.12
4	34.50	2.00	1.50	116.96	211.18
5	33.50	2.00	1.50	102.07	180.37
6	34.50	2.50	2.00	103.51	186.89
7	34.00	1.50	1.50	132.83	248.13
8	34.50	2.00	2.50	116.96	211.18
9	33.50	1.50	2.00	115.22	203.61
10	34.00	2.50	2.50	113.98	204.25
11	33.50	2.00	2.50	102.07	180.37
12	34.00	2.00	2.00	117.94	220.32
13	34.00	1.50	1.50	132.83	248.13

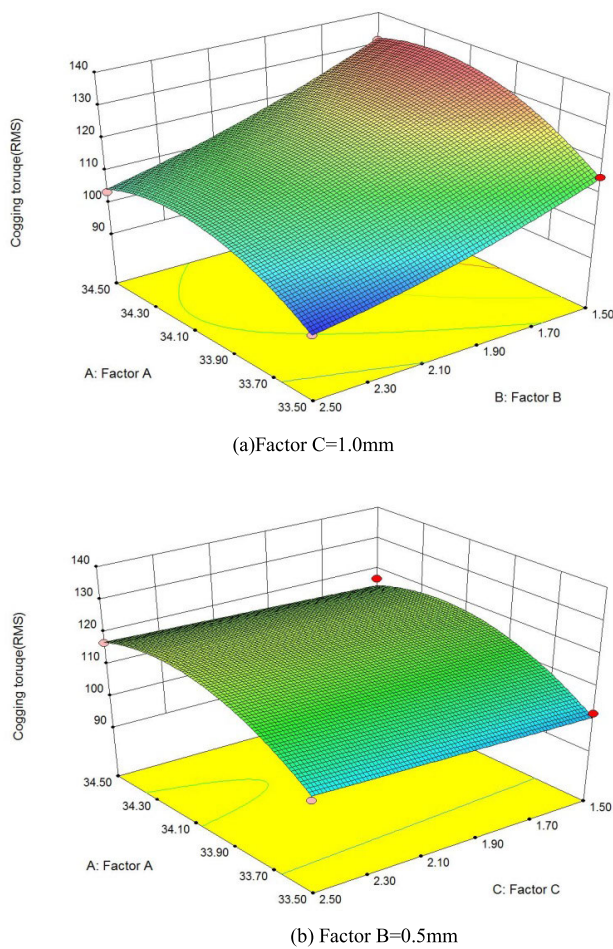


FIGURE 8. Response surface of RMS value of cogging torque.

In order to further explore the influence degree of each parameter on the objective function, the mean square error (MSE) and P value analysis were carried out. According to

the statistical theory, if the P value is less than 0.05, the factor has significant influence on the target parameter. If the P value is less than 0.01, the factor has extremely significant influence on the target parameter. The MSE and P value of each factor are displayed in Table 3. The response surface analysis results of 2 targeting parameters are shown in Fig. 8 and Fig.9.

It can be recognized from Fig.8 and Fig.9 that the RMS value increases first and then decreases with the increase of factor A. It reaches the maximum when the factor A is 34.2mm. When the factor A increases from 33.5mm to 34.2mm, the RMS value increases rapidly and when the factor A increases from 34.2mm to 34.5mm, the RMS value decreases slowly. The RMS value decreases linearly with the increase of factor B. In overall, the RMS value changes slowly along the direction of factor A, and decreases dramatically along the direction of factor B. This means factor B has a greater effect on the RMS value of cogging torque. As factor C increases, the RMS value increases slowly. The variation trend of the maximum cogging torque with each factor is basically consistent with the RMS of cogging torque, but it has a more widely variation range.

D. OPTIMAL SCHEME ANALYSIS

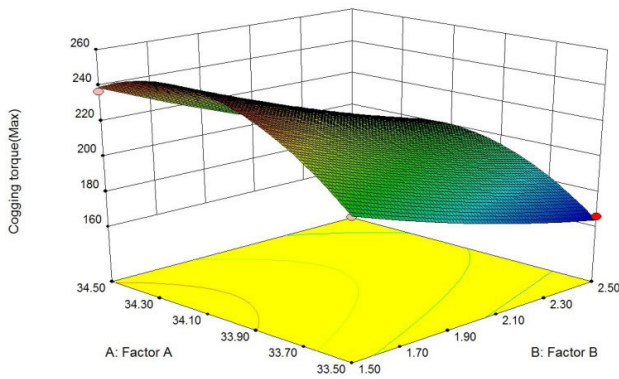
Based on the regression equations fitted by the response surface analysis, the RMS value and maximum value of cogging torque are taken as objective functions. The range of each factor is taken manufacturing process, operational safety and design experience into account. As results, the objective function and constraint conditions can be expressed as follows.

objective functions

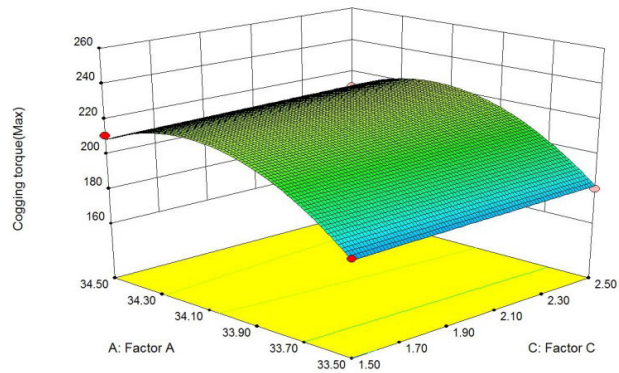
$$\begin{cases} \min T_{\text{cog-rms}}(\text{factorA}, \text{factorB}, \text{factorC}) \\ \min T_{\text{cog-max}}(\text{factorA}, \text{factorB}, \text{factorC}) \end{cases} \quad (12)$$

TABLE 3. Statistical analysis of response surface experiment results.

Factor	MSE		P value	
	RMS of cogging torque	Maximum of cogging torque	RMS of cogging torque	Maximum of cogging torque
A	386.98	1693.33	< 0.001	< 0.001
B	1175.64	4323.11	< 0.001	< 0.001
C	12.50	12.50	<0.0307	< 0.0870



(a) Factor C=1.0mm



(b) Factor B=0.5mm

FIGURE 9. Response surface of maximum value of cogging torque.

constraint conditions

$$\begin{cases} \text{factor A} \in [33.50\text{mm}, 34.50\text{mm}] \\ \text{factor B} \in [1.50\text{mm}, 2.50\text{mm}] \\ \text{factor C} \in [1.50\text{mm}, 2.50\text{mm}] \end{cases} \quad (13)$$

After calculation, when the factor A, factor B, and factor C are 33.51mm, 2.42mm, and 1.50mm, the RMS value and the maximum value of the cogging torque are the smallest.

V. VIBRATION MEASUREMENT EXPERIMENT

The vibration experiment was carried out to verify the correctness of the above theoretical analysis. A PMDCM with rectangular magnetic steel was manufactured depending on the optimal solution parameters. In addition, a reference motor was likewise manufactured. The factor A, factor B, and

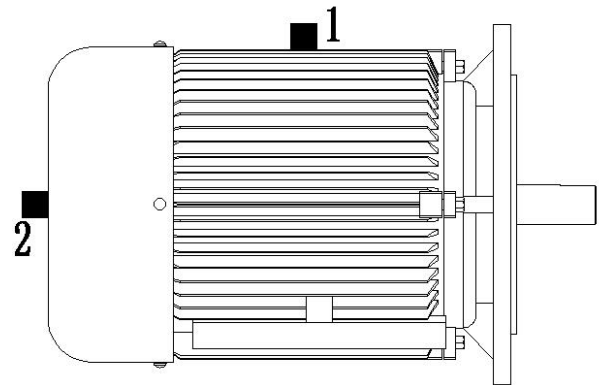


FIGURE 10. Measurement positions.

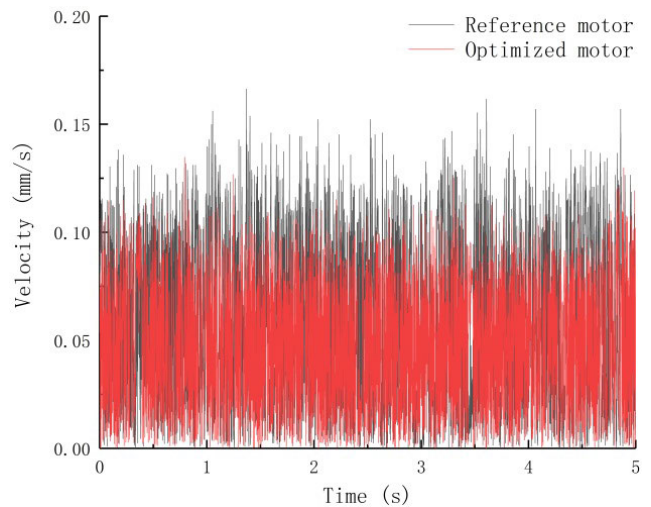


FIGURE 11. Vibration velocity of measuring point 1 of two motors.

factor C of the reference motor are 34.00mm, 1.50mm, and 2.00mm respectively. The other parameters of the two motors are same absolutely. Two positions of the motor displayed in Fig.10 are chosen for vibration testing.

The data acquisition card was used to measure the vibration velocity of two motors at the rated speed, and its measuring frequency is 500Hz. The numbers of channels are 16. The measuring range of velocity sensor is 0-20mm/s. The vibration velocity data of measurement point 1 and point 2 of the two motors are shown in Fig.11 and Fig.12 respectively. The maximum and average vibration velocity of two measuring points of two motors is displayed in Fig. 13.

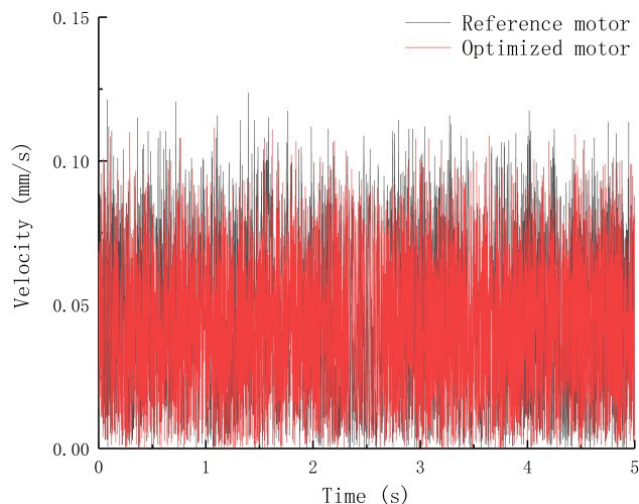


FIGURE 12. Vibration velocity of measuring point 2 of two motors.

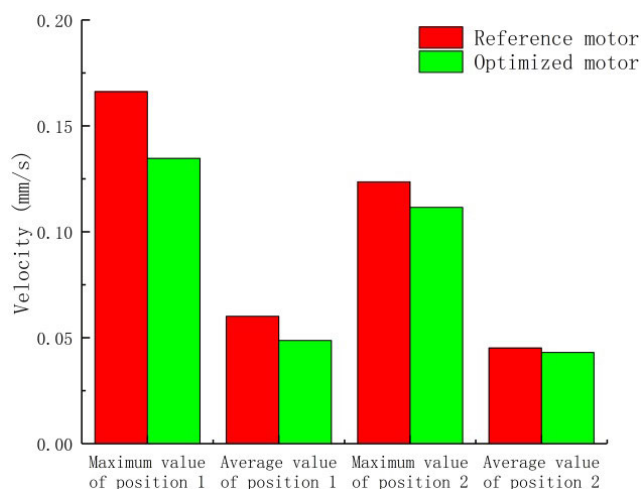


FIGURE 13. Maximum and average vibration velocity of two measuring points of two motors.

It can be known from Fig.11 and Fig.12 that the vibration velocity of the optimized motor is reduced obviously at point 1, but the vibration velocity reduction is smaller at measuring point 2. These results suggest that the cogging torque mainly affects the radial force and has little effect on the axial force. As is shown in Fig.13, the maximum and average data of vibration velocity of measuring point 1 are decreased by 18.99% and 19.03% respectively and the maximum and average vibration velocity of measuring point 2 are decreased by 9.73% and 4.70% respectively.

VI. CONCLUSION

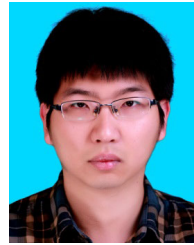
A new PMDCM of rectangular magnetic steel was designed and its vibration performance was optimized in this paper. The co-simulation of the designed motor was carried out based on RMxprt and MAXWELL. The output power, torque and transient magnetic field parameters were simulated and analyzed. The simulation results verify that the motor meets

the design requirements. Then the cogging torque of the designed motor was optimized by using response surface method. The influence degree of each factor on RMS value and maximum value of cogging torque was analyzed, and the optimal solution was calculated. When the factor A, factor B, and factor C are 33.51mm, 2.42mm, and 1.50mm respectively, the cogging torque is smallest. The fitting accuracy of the two regression equations is 94.30% and 97.26%. The influence degree of various factors on the cogging torque was clarified. At last, to verify the correctness of the analysis results, the optimized motor and reference motor were manufactured. And then the vibration velocity data of the two motors were measured. The measured data shows that the maximum and average data of vibration velocity at measuring point 1 are decreased by 18.99% and 19.03% and the maximum and average vibration velocity at measuring point 2 are decreased by 9.73% and 4.70%. That indicates that the cogging torque mainly affects the radial force and has little effect on the axial force. The radial vibration can be effectively reduced by optimizing the cogging torque. The method of vibration reduction in this paper is effective. Although the DC motor is taken as the research object, the research method also can be extended to AC motors. Therefore, this study makes a major contribution to research on vibration optimization by reducing cogging torque. The research methods and results in this paper have positive significance for the design of other permanent magnet motor.

REFERENCES

- [1] S. Cho, H. Ahn, H. C. Liu, H.-S. Hong, J. Lee, and S.-C. Go, "Analysis of inductance according to the applied current in spoke-type PMSM and suggestion of driving mode," *IEEE Trans. Magn.*, vol. 2, no. 99, Jun. 2017, Art. no. 8202404.
- [2] M. A. J. Kondelaji, E. F. Farahani, and M. Mirsalim, "Performance analysis of a new switched reluctance motor with two sets of embedded permanent magnets," *IEEE Trans. Energy Convers.*, vol. 12, no. 5, pp. 818–827, Jun. 2020.
- [3] M. Kimiabeigi, R. S. Sheridan, J. D. Widmer, A. Walton, M. Farr, B. Scholes, and I. R. Harris, "Production and application of HPMS recycled bonded permanent magnets for a traction motor application," *IEEE Trans. Ind. Electron.*, vol. 65, no. 5, pp. 3795–3804, May 2018.
- [4] J. Cha-Seung, K. Byung-II, and K. Ohbong, "Tolerance sensitivity analysis and robust optimal design method of a surface-mounted permanent magnet motor by using a hybrid response surface method considering manufacturing tolerances," *Energies*, vol. 11, no. 5, pp. 1159–1168, 2018.
- [5] J. Rahmani Fard and M. Ardebili, "Design and prototyping of the novel axial flux-switching permanent-magnet motor," *COMPEL Int. J. Comput. Math. Electr. Electron. Eng.*, vol. 37, no. 2, pp. 890–910, Mar. 2018.
- [6] E. F. Farahani, M. A. J. Kondelaji, and M. Mirsalim, "A new exterior-rotor multiple teeth switched reluctance motor with embedded permanent magnets for torque enhancement," *IEEE Trans. Magn.*, vol. 56, no. 2, pp. 1–5, Feb. 2020.
- [7] V. V. Grebenikov and M. V. Priymak, "Design of the electric motor with permanent magnets for electric vehicle according the driving cycle," *Tech. Electrodyn.*, vol. 18, no. 5, pp. 65–72, 2018.
- [8] Y.-P. Yang and M.-T. Peng, "A surface-mounted permanent-magnet motor with sinusoidal pulsewidth-modulation-shaped magnets," *IEEE Trans. Magn.*, vol. 55, no. 1, Jan. 2018, Art. no. 8100108.
- [9] Y.-P. Yang and M.-T. Peng, "A surface-mounted permanent-magnet motor with sinusoidal Pulsewidth-Modulation-Shaped magnets," *IEEE Trans. Magn.*, vol. 55, no. 1, pp. 1–8, Jan. 2019.
- [10] S. Wang, D. Peng, and Z. Wu, "Embedded position detection for permanent magnet synchronous motor with built-in magnets," *IEEE Sensors J.*, vol. 19, no. 21, pp. 9818–9825, Jan. 2019.

- [11] O. Ouledali, A. Meroufel, P. Wira, and S. Bentouba, "Direct torque fuzzy control of PMSM based on SVM," *Energy Procedia*, vol. 74, pp. 1314–1322, Aug. 2015.
- [12] Y. Wang and J. Fei, "Adaptive fuzzy sliding mode control for PMSM position regulation system," *Int. J. Innov. Comput., Inf. Control*, vol. 11, no. 3, pp. 881–891, Jun. 2015.
- [13] M. Seilmeier and B. Piepenbreier, "Sensorless control of PMSM for the whole speed range using two-degree-of-freedom current control and HF test current injection for low-speed range," *IEEE Trans. Power Electron.*, vol. 30, no. 8, pp. 4394–4403, Aug. 2015.
- [14] X. Chen, S. Yuan, and Z. Peng, "Nonlinear vibration for PMSM used in HEV considering mechanical and magnetic coupling effects," *Nonlinear Dyn.*, vol. 80, nos. 1–2, pp. 541–552, Apr. 2015.
- [15] I. A. A. Afinowi, Z. Q. Zhu, Y. Guan, J.-C. Mipo, and P. Farah, "Switched-flux machines with hybrid NdFeB and ferrite magnets," *COMPEL Int. J. Comput. Math. Electr. Electron. Eng.*, vol. 35, no. 2, pp. 456–472, Mar. 2016.
- [16] Y. Yang, A. Walton, R. Sheridan, K. Güth, R. Gauß, O. Gutfleisch, M. Buchert, B.-M. Steenari, T. Van Gerven, P. T. Jones, and K. Binnemans, "REE recovery from End-of-Life NdFeB permanent magnet scrap: A critical review," *J. Sustain. Metall.*, vol. 3, no. 1, pp. 122–149, Mar. 2017.
- [17] T. Turker, U. Buyukkeles, and A. F. Bakan, "A robust predictive current controller for PMSM drives," *IEEE Trans. Ind. Electron.*, vol. 63, no. 6, pp. 3906–3914, Jun. 2016.
- [18] H. W. Li, Y. T. Deng, and J. L. Wang, "Digital integration of PMSM speed controller based on FPGA," *Opt. Precis. Eng.*, vol. 23, no. 4, pp. 1105–1113, 2015.
- [19] J. Zou, S. Zhao, and X. Yang, "Optimization of cogging torque of external rotor PMSM based on genetic algorithm," *Small Special Elect. Mach.*, vol. 48, no. 4, pp. 1–6, 2020.
- [20] W. Mingxing, "A way of optimizing cogging torque to reduce vibration and noise for permanent magnet synchronous motor," *Electr. Mach. Control Appl.*, vol. 44, no. 2, pp. 110–115, 2017.
- [21] Z. Chen, K. S. Huang, and Y. F. Tian, "Research on cogging torque of permanent magnet synchronous motor with integer slot," *Explosion-Proof Electr. Mach.*, vol. 49, no. 1, pp. 10–15, 2014.
- [22] T. Tarczewski and L. M. Grzesiak, "Constrained state feedback speed control of PMSM based on model predictive approach," *IEEE Trans. Ind. Electron.*, vol. 63, no. 6, pp. 3867–3875, Jun. 2016.
- [23] F. Colamartino, C. Marchand, and A. Razek, "Torque ripple minimization in permanent magnet synchronous servodrive," *IEEE Trans. Energy Convers.*, vol. 14, no. 3, pp. 616–621, Sep. 1999.
- [24] J.-X. Xu, S. K. Panda, Y.-J. Pan, T. H. Lee, and B. H. Lam, "A modular control scheme for PMSM speed control with pulsating torque minimization," *IEEE Trans. Ind. Electron.*, vol. 51, no. 3, pp. 526–536, Jun. 2004.
- [25] G. Zenginobuz, I. Cadirci, M. Ermis, and C. Barlak, "Performance optimization of induction motors during voltage-controlled soft starting," *IEEE Trans. Energy Convers.*, vol. 19, no. 2, pp. 278–288, Jun. 2004.



KAI HU was born in Kuiwen, Weifang, Shandong, China, in 1990. He received the B.S. and M.S. degrees in vehicle engineering from the Shanghai University of Engineering Science, in 2015. He is currently pursuing the Ph.D. degree with Nanjing Tech University.

Since 2015, he has been a Research Assistant with the Nanjing Institute of Agricultural Mechanization. He is the author of more than 120 articles and more than 15 patents. His research interests include the controlling technology of vibration and noise of permanent magnetic motors.

Dr. Hu won the National Scholarship for graduate students in 2015.



GUANGMING ZHANG was born in Jiangdu, Yangzhou, Jiangsu, China, in 1965.

From April 2006 to August 2006, he was a Senior Visiting Scholar with Concordia University, Canada. He is currently a Ph.D. Supervisor. He is also the Executive Vice President of the Graduate School, Nanjing Tech University. He is the author of three books, more than 160 articles, and 16 patents. His main research interests include intelligent control theory and application, and electromechanical system integrated control.

Prof. Zhang is the Vice Chairman of the China Electrotechnical Society and the Director of the China Association for the Application of Electromechanical Integration Technology.

...